TECHNIQUES

Quantitative single-molecule imaging of TLR4 reveals ligand-specific receptor dimerization

Carmen L. Krüger,[1] Marie-Theres Zeuner,[2] Graeme S. Cottrell,[3] Darius Widera,[2] Mike Heilemann[1]*

In humans, invading pathogens are recognized by Toll-like receptors (TLRs). Upon recognition of lipopolysaccharide (LPS) derived from the cell wall of Gram-negative bacteria, TLR4 dimerizes and can stimulate two different signaling pathways, the proinflammatory, MyD88-dependent pathway and the antiviral, MyD88-independent pathway. The balance between these two pathways is ligand-dependent, and ligand composition determines whether the invading pathogen activates or evades the host immune response. We investigated the dimerization behavior of TLR4 in intact cells in response to different LPS chemotypes through quantitative single-molecule localization microscopy. Quantitative superresolved data showed that TLR4 was monomeric in the absence of its co-receptors MD2 and CD14 in transfected HEK 293 cells. When TLR4 was present together with MD2 and CD14 but in the absence of LPS, 52% of the receptors were monomeric and 48% were dimeric. LPS from *Escherichia coli* or *Salmonella minnesota* caused the formation of dimeric TLR4 complexes, whereas the antagonistic LPS chemotype from *Rhodobacter sphaeroides* maintained TLR4 in monomeric form at the cell surface. Furthermore, we showed that LPS-dependent dimerization was required for the activation of NF-κB signaling. Together, these data demonstrate ligand-dependent dimerization of TLR4 in the cellular environment, which could pave the way for a molecular understanding of biased signaling downstream of the receptor.

INTRODUCTION

Toll-like receptors (TLRs) are pattern recognition receptors, which play a pivotal role in the innate immune response and recognize danger-associated (or damage-associated) molecular patterns (DAMPs) and pathogen-associated molecular patterns (*1*). The most studied receptor among the TLR family is TLR4, which has as its canonical ligand lipopolysaccharide (LPS), a major component of the cell wall of Gram-negative bacteria (*2*, *3*). TLR4 is a transmembrane receptor, comprising an extracellular domain that is connected to the intracellular domain by a leucine-rich repeat motif. LPS is first recognized by the LPS-binding protein (LBP) (*4*, *5*). Subsequently, the TLR4 co-receptor CD14 (cluster of differentiation 14) transfers LPS to the extracellular TLR4–MD2 (myeloid differentiation protein 2) heterodimer. This TLR4-MD2 heterodimer then dimerizes with another TLR4-MD2 complex and recruits specific intracellular adaptor molecules to promote the activation of downstream signaling pathways. A unique feature of TLR4, compared to other TLRs, is its ability to activate two distinct signaling pathways: the myeloid differentiation primary response gene 88 (MyD88)–dependent pathway and the MyD88-independent pathway (*6*, *7*). Both pathways result in the activation of nuclear factor κB (NF-κB) signaling, but only the MyD88-independent pathway stimulates signaling by interferon regulatory factor 3 (IRF3) (*8*–*11*). It is well understood that MD2 is necessary for TLR4 signaling and especially for the dimerization of TLR4 in the receptor complex, whereas the role of CD14 in the dimerization process is less well defined (*12*–*14*).

LPS is composed of three major components: an O side chain, a core oligosaccharide, and lipid A (*15*, *16*). The lipid A moiety is a very diverse molecule and differs structurally depending on the bacterial strain from which the LPS is derived. Lipid A from *Escherichia coli* LPS (LPS_{EC}) is hexa-acylated, whereas lipid A from *Salmonella minnesota* LPS (LPS_{SM}) is hepta-acylated (*16*, *17*). In contrast, the lipid A moiety from *Rhodobacter sphaeroides* LPS (LPS_{RS}) is penta-acylated and antagonizes the receptor (*18*, *19*). These acylation patterns in different LPS chemotypes not only affect the agonistic properties of LPS but also result in biased signaling in the glioma cell line U251. In these cells, LPS_{EC} induces a substantial inflammatory response through NF-κB, whereas LPS_{SM} is less proinflammatory and has a greater stimulatory effect on IRF3 signaling (*20*). In addition, differences in downstream signaling do not depend on the formation of larger clusters of TLR4 (*20*). How LPS_{RS} binds to LBP, CD14, and MD2 is less well understood; however, the dimerization of two TLR4-MD2 complexes is inhibited and signaling is abrogated (*21*, *22*). Here, we investigated the ligand-induced dimerization of TLR4 in intact cells using quantitative single-molecule localization microscopy (SMLM).

SMLM is a powerful tool that is used to investigate cellular structures in situ that have a spatial resolution well below the diffraction limit of light microscopy (*23*). Single fluorescent emitters are separated over time, and their localizations are determined with high precision. The reconstruction of the molecular coordinates results in a superresolved image, giving insights into the nanoscale organization of the target cellular structure. SMLM requires photoactivatable or photoswitchable fluorophores, which can be either fluorescent proteins (FPs), such as those used in photoactivated localization microscopy (PALM), or organic fluorophores, such as those used in (direct) stochastic optical reconstruction microscopy (STORM or *d*STORM) (*24*–*26*). SMLM is particularly suited to the study of membrane proteins, and it provides information on nanoscale cluster size, distribution, and molecular numbers (*27*–*29*).

Robust quantitative information can be obtained from SMLM data if proteins are labeled stoichiometrically, which can be achieved through the conjugation of a photoactivatable FP (paFP) to the protein of interest (*30*). A common paFP for this purpose is mEos2, which is photoconvertible from a green to an orange form after irradiation with ultraviolet (UV) light (*31*). Advanced SMLM concepts, which, in addition to localizing single fluorophores, make use of the intrinsic "blinking" of paFPs, even enable the prediction of copy numbers from

[1]Institute of Physical and Theoretical Chemistry, Goethe University, Max von Laue Straße 7, 60438 Frankfurt/Main, Germany. [2]Stem Cell Biology and Regenerative Medicine, School of Pharmacy, University of Reading, Hopkins Building, Whiteknights, Reading RG6 6UB, UK. [3]Cellular and Molecular Neuroscience, School of Pharmacy, University of Reading, Hopkins Building, Whiteknights, Reading RG6 6UB, UK.
*Corresponding author. Email: heilemann@chemie.uni-frankfurt.de

protein clusters that cannot be resolved with superresolution SMLM and thus can provide insight into the oligomeric state of a membrane protein (*32–34*). Because oligomerization is often the starting point that initiates signaling pathways mediated by receptors, the quantitative information obtained in situ is highly relevant (*35–37*).

Here, we applied quantitative SMLM imaging to determine the oligomeric state of TLR4 in situ. We focused on the resting receptor and the roles of the co-receptors MD2 and CD14 and explored how LPS from different bacterial species influenced the ratio between the monomeric and dimeric forms of the receptor. Clustering of TLR4 on the plasma membrane in response to LPS is controversially discussed (*20*, *38*). However, investigations on higher-order clustering of TLR4 with the help of conventional SMLM techniques are not sensitive enough to decipher monomeric TLR4 from dimeric TLR4.

Using SMLM, we distinguished between monomeric TLR4 in the absence of CD14 and MD2 and a mixed population of monomeric and dimeric TLR4 in their presence. We found a correlation between dimerization of TLR4 and agonistic LPS, whereas the penta-acylated, antagonistic LPS_{RS} favored monomeric TLR4. To demonstrate the functionality of the TLR4_mEos2 construct in human embryonic kidney (HEK) 293 cells, we performed NF-κB gene reporter assays and observed increased NF-κB activity in response to agonistic LPS forms, but no increase in NF-κB activity in response to LPS_{RS} was observed. In addition, we did not detect differential activation patterns of NF-κB and IRF3 in HEK 293 cells expressing TLR4_mEos2 after exposure to different agonistic LPSs. Finally, higher-order oligomerization of TLR4 was not observed after treatment with LPS.

RESULTS

Quantitative SMLM of calibration proteins

We used SMLM and quantitative analysis to determine the oligomeric state of TLR4 in clusters consisting of the TLR4-MD2 complex in cells. For this experimental approach, an SMLM image stack of a cellular target protein labeled with a paFP was recorded, from which a superresolved image was generated (Fig. 1A). Typically, a single paFP emits multiple times during an imaging experiment (and before it undergoes photodestruction), which appears as so-called blinking or reoccurrence of fluorescence events (Fig. 1A). This blinking behavior is described by simple kinetic equations; a simple yet robust analysis approximates the histogram of the blinking events with an appropriate model function (see Fig. 1A and Materials and Methods) (*34*, *39*). The strength of this quantitative approach is that information about the stoichiometry of proteins within single-protein clusters can also be obtained: Although the individual proteins within a protein cluster cannot be resolved optically even with superresolution microscopy, the blinking pattern of the paFPs conjugated to these proteins changes with respect to the number of protein units. An accurate analysis requires that a target protein is labeled stoichiometrically, for example, with a paFP. The analysis of blinking cycles also accounts for FPs that are not detected, for instance, through misfolding, premature bleaching, etc. (see Fig. 1 and Materials and Methods for a detailed description of the experimental approach) (*31*, *40–42*). Analyzing the blinking pattern from about 100 clusters is statistically sufficient to determine the oligomerization state of mEos2-tagged membrane proteins (*39*).

Here, we used quantitative SMLM to determine the oligomeric state of TLR4 under different cellular conditions. More specifically, we analyzed the fraction of monomeric and dimeric TLR4 on the plasma membrane of HEK 293 cells. We first performed calibration experiments in HEK 293 cells by expressing two proteins of known stoichiometry, namely, CD86 and cytotoxic T lymphocyte–associated protein–4 (CTLA-4), which are known to be monomeric and dimeric proteins, respectively (*34*, *43–46*). Both proteins were expressed in HEK 293, and PALM images were acquired. CD86_mEos2 showed individual clusters, which were uniformly distributed on the cell surface (Fig. 1B). To determine the oligomeric state of CD86_mEos2, we performed a blinking distribution analysis and generated a histogram of the relative frequency distribution of blinking events (herein referred to as blinking number distribution) (Fig. 1C). As expected, CD86_mEos2 showed a clear monomeric distribution, which was very well approximated by the corresponding fit function (Fig. 1C) (*34*). This fit function returned the value $p = 0.32$ (which reports on the fraction of mEos2 molecules that did not blink), which is in good accordance with published values for CD86_mEos2 in other cell lines (*34*). The same procedure was performed for CTLA-4_mEos2. Superresolved images showed a uniform distribution of clusters at the cell surface (Fig. 1D) and a distribution of blinking events (Fig. 1E) that was very well approximated by a dimeric model. In addition to the p value, this model reports on the fraction of molecules that was not detected (for example, because of photodamage or misfolding), which we termed q and had the value $q = 0.29$ (Table 1). This value reflects a detection efficiency of mEos2 of 71%, which is in good agreement with the detection efficiencies of mEos2 in similar experiments (*41*, *47*). We determined the experimental localization precision of our SMLM experiments to be 15.1 ± 0.4 nm for CD86_mEos2 and 16.1 ± 1.0 nm for CTLA-4_mEos2 using a nearest-neighbor analysis (NeNA) (Table 1) (*48*). This translates into a spatial resolution of about 50 nm (assuming two point objects), which is not sufficient to resolve individual proteins within a protein cluster (*49*).

Dimerization of TLR4 in HEK 293 cells

Next, we investigated the proportion of monomers and dimers of TLR4 in resting HEK 293 cells. These cells represent an excellent model system in which to study TLR4 signaling because they lack endogenous TLR4, CD14, and MD2; however, they have the necessary intracellular signaling components required for the MyD88-dependent pathway, but not for the MyD88-independent pathway (*6*). We recorded superresolved images of HEK 293 transfected with plasmid encoding TLR4_mEos2 and selected for analysis only those cells that exhibited fewer than 4 protein clusters/μm^2 of the plasma membrane, which is in the same range as the copy numbers of endogenous TLR4 in U251 cells (*20*). This selection criterion likely ensured that dimerization as a result of protein overexpression was largely excluded from the analysis. At the same time, errors in the analysis because of an increasing number of overlapping protein clusters in the microscopy images were minimized. We analyzed the blinking number distributions of TLR4_mEos2 generated under different experimental conditions, which we approximated with suitable model functions that reported on the proportions of monomeric and dimeric TLR4 (Fig. 2A).

First, we investigated the stoichiometry of TLR4_mEos2 clusters in the absence of CD14 and MD2. HEK 293 cells were transiently transfected with plasmid encoding TLR4_mEos2, superresolved images were acquired, and the blinking distribution was generated. In the absence of CD14 and MD2, we found that TLR4 exclusively formed monomers (Fig. 2B). We determined a p value of 0.31, which is very similar to the p value that we observed in the calibration experiment with CD86 (Fig. 1C). In HEK 293 cells that stably expressed TLR4_mEos2 with CD14 and MD2, the blinking distribution of TLR4_mEos2 was consistent with the presence of both monomeric (52%) and dimeric

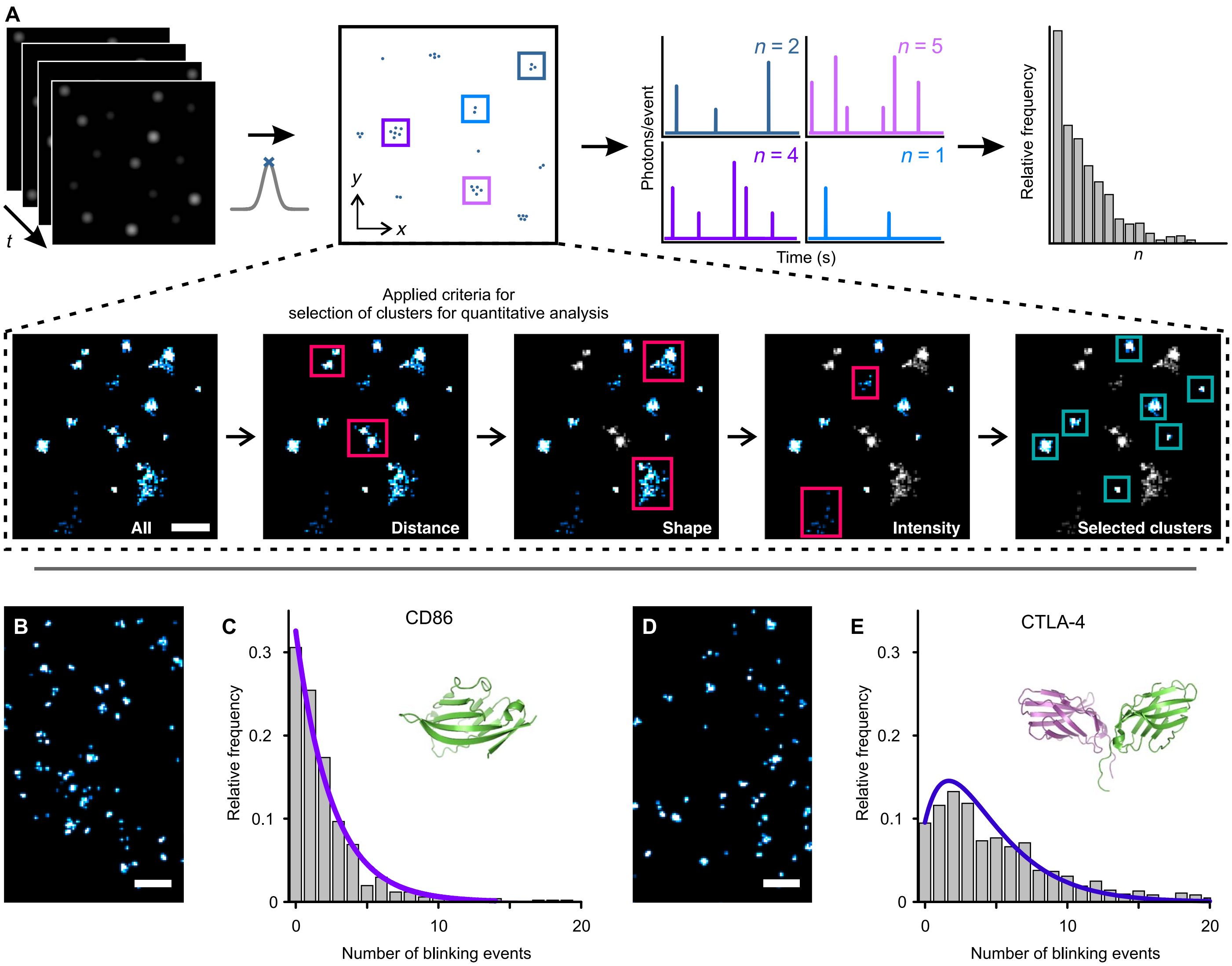

Fig. 1. Single-molecule, superresolution imaging of membrane protein clusters and determination of protein stoichiometry in protein clusters. (**A**) A superresolved SMLM image is generated from a stack of images by determining the position of each molecule with nanometer precision. From the superresolved image, single clusters are selected, and the number of fluorescence bursts within each cluster is determined. The number of blinking events, which is the number of fluorescence bursts minus one, is plotted as a histogram and provides information on the average molecule count within the protein clusters. The selection of clusters for quantitative analysis is based on the superresolved image and removes overlapping clusters, clusters with irregular shape or size, or clusters that are composed of only very few points (pink boxes). Selected clusters (cyan boxes) were further analyzed. Illustration of these selection criteria is demonstrated for dimeric CTLA-4_mEos2. (**B** and **C**) PALM image (B) of HEK 293 cells expressing the monomeric protein CD86_mEos2 [inset, Protein Data Bank (PDB): 1NCN] in the plasma membrane and the blinking distribution (C) with fit function. (**D** and **E**) PALM image (D) of HEK 293 cells expressing the dimeric protein CTLA-4_mEos2 (inset, PDB: 3OSK) in the plasma membrane and the blinking distribution (E) with fit function. Scale bars, 200 nm. Data are from at least 500 clusters from at least nine cells recorded in at least three independent experiments.

Table 1. Values for the calibration proteins used for quantitative SMLM. Determination of the parameters *p* and *q* derived from the quantitative analysis of the blinking number distributions for the calibration proteins CD86_mEos2 and CTLA-4_mEos2. The average localization precision calculated with a NeNA is shown. Data are means ± SEM.

	p	q	N_{cells}	$N_{analyzed\ clusters}$	Average localization precision (nm)
CD86_mEos2	0.32	—	9	504	15.1 ± 0.4
CTLA-4_mEos2	—	0.29	10	844	16.1 ± 1.0

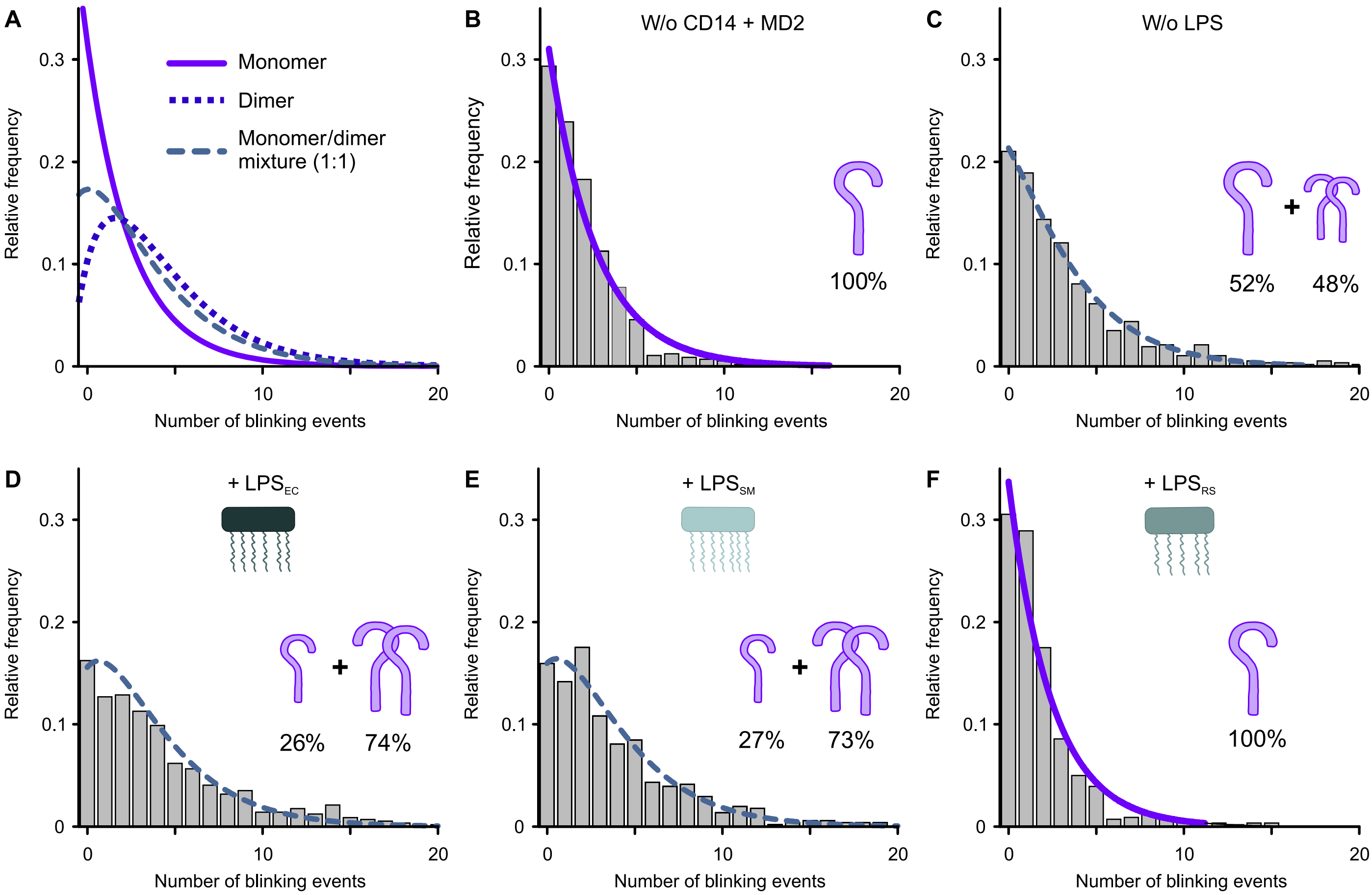

Fig. 2. Stoichiometry analysis of TLR4_mEos2 in HEK 293 cells in situ. (**A**) Model-derived fit functions describing the blinking histogram for a protein monomer (purple), dimer (violet), and a weighted average of monomer and dimer in equal parts (blue). See Materials and Methods for further details. (**B**) Analysis of the distribution of blinking events in HEK 293 cells transiently transfected with plasmid encoding TLR4_mEos2 but lacking the co-receptors CD14 and MD2. We calculated the parameter p, which reports on the fraction of molecules that did not blink, as $p = 0.31$. (**C**) Analysis of blinking events in HEK293_CD14MD2 cells that were transfected with plasmid encoding TLR4_mEos2 but were not treated with LPS. TLR4 was found in a mixed population of monomers (52%) and dimers (48%). $p = 0.32$, $q = 0.29$. (**D** to **F**) HEK293_CD14MD2 cells transfected with plasmid encoding TLR4_mEos2 were treated with LPS$_{EC}$ (D), LPS$_{SM}$ (E), or LPS$_{RS}$ (F), and then, the distribution of blinking events was determined. (D) Treatment with LPS$_{EC}$ induced a weighted average of monomeric (26%) and dimeric (74%) TLR4 (used values: $p = 0.32$, $q = 0.29$). (E) For treatment with LPS$_{SM}$, 27% monomers and 73% dimers were detected (used values: $p = 0.32$, $q = 0.29$). (F) Treatment with LPS$_{RS}$ led to monomeric TLR4 only ($p = 0.33$). Data are from at least 500 clusters from at least nine cells recorded in at least three independent experiments.

(48%) TLR4 (Fig. 2C). These results support the importance of the co-receptors CD14 and MD2 in enabling TLR4 dimerization (*12*, *13*). However, it cannot be excluded that this dimerization was the result of the activation of TLR4 signaling by endogenous ligands.

We next investigated how different LPS chemotypes influenced the dimerization behavior of TLR4. We used a cell line stably expressing CD14 and MD2 (HEK293_CD14MD2 cells) and performed transient transfection of these cells with plasmid encoding TLR4_mEos2. These HEK293_CD14MD2_TLR4mEos2 cells were treated with LPS derived from *E. coli*, *S. minnesota*, or *R. sphaeroides*; superresolved SMLM images were acquired; and the blinking distributions were analyzed (Fig. 2, D to F). Each of the various chemotypes of LPS resulted in a uniform distribution of TLR4 on the cell surface, and no formation of larger clusters was observed, which is consistent with a previous study (*20*). The blinking distributions generated in response to LPS$_{EC}$ and LPS$_{SM}$ were consistent with mixed populations of monomeric and dimeric TLR4 (Fig. 2, D and E). In comparison to untreated cells (Fig. 2C), both LPS$_{EC}$ and LPS$_{SM}$ induced the formation of dimeric TLR4 (Fig. 2, D and E). LPS from *R. sphaeroides* is a well-known antagonist of TLR4 signaling; therefore, we used it to investigate the oligomerization behavior of TLR4 under antagonistic influence (*19*). The blinking distribution exclusively showed monomers of TLR4 (Fig. 2F) and was distinct from the distributions caused by LPS$_{SM}$ or LPS$_{EC}$ (Fig. 2, D and E).

We next performed gene reporter assays to assess the functionality of the fluorescently tagged TLR4 constructs (Fig. 3A). Here, we cotransfected HEK293_CD14MD2 cells with an NF-κB–dependent luciferase reporter gene and plasmids encoding TLR4_GFP, TLR4_mEos2, or enhanced green fluorescent protein (EGFP). In the absence of LPS, we observed an increase in NF-κB activity in cells expressing TLR4_GFP or TLR4_mEos2 compared to that in cells expressing EGFP alone. The functionality of the exogenous receptor was confirmed in experiments in which LPS$_{EC}$ caused a substantial increase in NF-κB activity in cells expressing TLR4_GFP or TLR4_mEos2 but not in cells expressing EGFP alone.

We then investigated intracellular signaling activation in experiments in which HEK293_CD14MD2 cells were cotransfected with plasmids

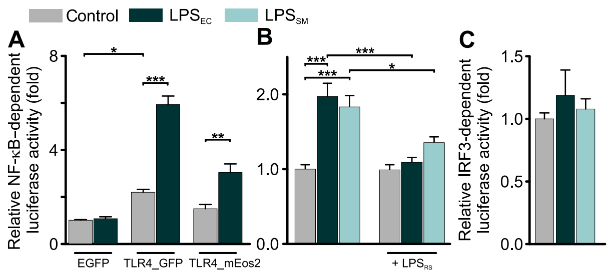

Fig. 3. Measurement of NF-κB– and IRF3-dependent luciferase activities to determine the potencies of different LPS chemotypes and the functionality of TLR4_mEos2. (**A** to **C**) HEK293_CD14MD2 cells were transiently transfected with (A) plasmids encoding EGFP, TLR4_GFP, or TLR4_mEos2 and an NF-κB–dependent luciferase reporter plasmid, (B) plasmid encoding TLR4_mEos2 together with the NF-κB–dependent luciferase reporter plasmid, or (C) plasmid encoding TLR4_mEos2 together with the IRF3-dependent luciferase reporter plasmid. Luciferase activity was detected in (A) unstimulated and LPS_{EC}-stimulated cells; (B) untreated cells (control) and in cells stimulated with LPS_{EC} or LPS_{SM} in the absence or presence of LPS_{RS}, as indicated; or (C) treated with LPS_{EC} or LPS_{SM} or left untreated (control). Intensity values were normalized to (A) untreated EGFP-expressing cells or (B and C) control cells. Data are means ± SEM of at least three experiments. *$P < 0.05$, **$P < 0.01$, ***$P < 0.001$ by one-way analysis of variance (ANOVA) followed by Bonferroni correction.

encoding TLR4_mEos2 and an NF-κB–dependent luciferase reporter. Treatment of these cells with LPS_{EC} or LPS_{SM} resulted in a substantial increase in NF-κB–dependent luciferase activity compared to that in untreated cells (Fig. 3B). Together with the data obtained from quantitative SMLM, these findings show a correlation between dimerization and signaling through TLR4. This finding is also consistent with the NF-κB activity measured in response to LPS_{RS}, where no statistically significant difference compared to that in control cells was observed (Fig. 3B). Furthermore, LPS_{RS} prevented NF-κB activation in cells treated simultaneously with either LPS_{EC} or LPS_{SM} (Fig. 3B). The concentrations of LPS_{RS} used in this study were chosen to completely inhibit TLR4 dimerization and signaling (*22*). A study showed that LPS_{EC} and LPS_{SM} exhibit functional selectivity in U251 glioma cells, promoting differential activation of NF-κB and IRF3 (*20*). In these U251 cells, LPS_{EC} had a more substantial effect on NF-κB signaling than on IRF3 signaling, whereas the reverse was true for LPS_{SM}. Therefore, we investigated whether LPS_{EC} and LPS_{SM} were similarly capable of biased signaling in HEK293_CD14MD2 cells cotransfected with plasmids encoding TLR4_mEos2 and an IRF3 reporter. However, we were unable to detect any substantial changes in IRF3 activity in response to either LPS_{EC} or LPS_{SM}, similar to control cells (Fig. 3C).

DISCUSSION

We used quantitative SMLM to determine the different oligomerization states of TLR4_mEos2 in HEK 293 cells in situ. We specifically investigated how TLR4 oligomerizes in the presence and absence of the co-receptors MD2 and CD14 and in response to different LPS chemotypes. Quantitative SMLM makes use of the observation that single fluorophores show blinking, namely, reoccurrence of a fluorescence signal over time. This blinking follows kinetic equations, and as such, the analysis of blinking distributions enables information about the number of fluorophores within a spot to be extracted. This analysis also accounts for the incomplete photodetection of fluorophores (q value; see Materials and Methods). Here, we used the paFP mEos2 for quantitative SMLM of TLR4 in HEK 293 cells and analyzed the oligomeric states of TLR4_mEos2 protein clusters in the plasma membrane.

An important validation of quantitative SMLM is to analyze the blinking distribution of calibration proteins that are exclusively monomeric or dimeric. We used monomeric CD86 and dimeric CTLA-4 and validated their oligomeric state in HEK 293 cells. The fit produced results (blinking probability, $p = 0.31$; fraction of undetected molecules, $q = 0.29$) that were consistent with values determined for these two proteins in other cell lines (*34*). Note that quantitative SMLM requires criteria for the selection of protein clusters that are analyzed (see Fig. 1A and Materials and Methods). Superresolved protein clusters that, for example, are either too close to a second protein cluster or exhibit an irregular shape must be excluded, and the cellular background signal and membrane curvature generate challenges for this kind of superresolution microscopy (*50*, *51*). This could be addressed in the future by the development of more sophisticated image analysis tools that are able to resolve overlapping protein clusters and that can perform in the presence of a high background signal.

The cluster selection procedure that we used for this study excluded large clusters from our analysis. We focused on the distribution of TLR4 monomers and dimers and how this distribution was affected by LPS. It should be noted that in our current study, we did not observe clusters of TLR4 in the PALM images that would indicate a higher-order clustering of the receptor or clusters larger than 80 nm in radius. Another concern is the use of a sufficient number of clusters needed to generate a statistically meaningful blinking number distribution. Here, we selected at least 500 protein clusters for analysis from at least nine individual cells (for each condition), which largely exceeds the theoretical prediction of at least 100 protein clusters needed for a robust determination of the oligomeric state (*39*).

We next investigated the dimerization behavior of TLR4 in response to different LPS chemotypes. All superresolved images of TLR4_mEos2 displayed no visible differences in the cluster sizes on intact cells, and no formation of clusters larger than 80 nm in radius was observed. This finding is consistent with a study that investigated the clustering of TLR4 on glioma cells using immunostaining and *d*STORM imaging and reported a cluster size of about 60 nm for TLR4 in response to either LPS_{EC} or LPS_{SM} (*20*). In contrast to these findings, another study reported a large-scale clustering of TLR4 in response to LPS_{EC} (*38*). The discrepancies between the studies performed by Aaron *et al.* (*38*) and Zeuner *et al.* (*20*) may be explained by the use of different cell lines and different experimental procedures. First, Aaron *et al.* investigated TLR4 in mouse macrophage-like cells with immunofluorescence labeling (*38*), and discrepancies in the cluster sizes of TLR4 could be the result of different behaviors of mouse and human TLR4 (hTLR4) (*52*). Second, SMLM imaging with organic fluorophores requires high laser intensities to ensure efficient photoswitching and thus optimal imaging conditions, and it requires careful adjustment of the imaging conditions (*53*). Finally, it is also possible that HEK 293 cells do not support the formation of large TLR4 clusters; however, large receptor clusters were reported for the epidermal growth factor receptor and the β_2-adrenergic receptor (*54*, *55*). Nevertheless, both studies were not sensitive enough to decipher the dimerization behavior of TLR4 (*20*, *38*).

Here, we analyzed TLR4 oligomerization in situ and performed quantitative SMLM imaging of TLR4 before and after treatment with different LPS chemotypes, as well as with and without MD2 and CD14 in HEK 293 cells. These cells represent an excellent model in which to study TLR4 signaling because they lack endogenous TLR4 but also

TLR2, which activates MyD88-dependent signaling through other pathogen-derived molecules (that are often present in low-purity LPS preparations) (*56*). Investigations of the oligomerization behavior of TLR4 under different experimental settings enabled us to propose a model for the activation and dimerization of TLR4. Consistent with previous data, we observed that in the absence of MD2 and CD14, TLR4 was found exclusively as a monomer at the cell surface in HEK 293 cells (*12*, *13*). When TLR4 was expressed together with MD2 and CD14, we detected a substantial switch with the appearance of TLR4 dimers. The existence of dimers in the absence of LPS might be explained by the activation of the receptor with as yet undefined endogenous ligands or DAMP-like proteins (*18*). Our luciferase activity assays inferred that these dimers were active because the presence of CD14 and MD2 (rather than EGFP) in HEK cells expressing TLR4 was sufficient to promote NF-κB activation (Fig. 3). We hypothesize that this could be due to potential DAMP-like proteins, such as heat shock proteins, β-defensin, or HMGB1 (high-mobility group box 1), which may have been present in the culture medium or signaled through the activation of intracellular TLR4 (*18*). The binding of endogenous ligands to TLR4 is a matter of an ongoing scientific debate and thus cannot be excluded as a factor responsible for the dimeric fraction of TLR4 (*57*, *58*). Functional selectivity of LPS_{EC} and LPS_{SM} was tested in HEK293_CD14MD2 cells transfected with plasmid encoding TLR4_mEos2 using an IRF3-biased signaling assay. However, none of the different LPS chemotypes stimulated any substantial increased in IRF3 activity. HEK 293 cells have low amounts of TIR domain–containing adaptor-inducing interferon-β (TRIF), which is an essential intracellular adaptor protein that promotes the TLR4-stimulated, MyD88-independent activation of IRF3 (*59*). A study examining IRF3 activation in HEK 293 cells used cells transfected with plasmid encoding TRIF to circumvent this problem (*6*). Although the downstream signaling events were not the primary aim of our study here, it would be interesting to investigate which intracellular signaling proteins are required to induce biased signaling by TLR4.

After applying different LPS chemotypes to TLR4, the ratios of monomeric and dimeric complexes changed. LPS_{SM} and LPS_{EC} resulted in mainly dimeric TLR4 (73 and 74%, respectively). Nevertheless, monomeric TLR4 was also present on the plasma membrane, which might be explained by the recycling of TLR4 back to the plasma membrane or the incomplete occupancy of TLR4 complexes by LPS. In contrast, LPS_{RS} resulted in only monomeric TLR4 and an NF-κB activity similar to that in unstimulated cells. Note that there was no direct relationship between the dimerization of TLR4 and NF-κB activity, especially in the case of treatment with LPS_{RS}. In untreated cells, we readily detected dimeric TLR4 at the cell surface; however, the extent of NF-κB activation was similar to that observed in cells in which no dimers were detectable in response to LPS_{RS} (Fig. 3B). Because we know of no evidence of the activity of TLR4 dimers that exists under basal conditions, we hypothesize that the basal activity in each case is due solely to intracellular TLR4 activity, with no stimulation of NF-κB activity by cell surface receptors. In support of this hypothesis, TLR4 is found in the cytoplasm of dendritic cells and can be activated by intracellular *Neisseria meningitidis* (*60*). Moreover, in macrophages, intracellular TLR4 signaling leads to an increase in the abundance of *MCP-1* mRNA, an NF-κB target gene, which suggests that intracellular TLR4 is functional (*61*). We suggest that intracellular TLR4 activation in transfected HEK 293 cells could be stimulated by endogenous intracellular ligands (for example, heat shock proteins). It is unlikely that this intracellular signaling would be affected by LPS_{RS}, and this could explain why LPS_{RS}, although it led to the maintenance of TLR4 monomers at the cell surface, did not affect the basal NF-κB activity observed in untreated cells. Overall, our results are in agreement with the data describing the prevention of dimerization and signaling behavior of TLR4 upon treatment with antagonistic ligands (*21*).

A photobleaching study of the dimerization of TLR4 reported similar results to ours (*62*). Briefly, Yang *et al.* showed that 87.5% of TLR4 was monomeric, whereas 12.5% of TLR4 was dimeric in cells in the absence of LPS (*62*). After treatment with LPS_{EC}, the distribution changed to 48.3% monomeric and 51.7% dimeric. However, photobleaching is a diffraction-limited method that is often hampered by the fact that only sparse samples can be investigated (less than 2 particles/μm^2) (*63*). This fact might explain the different distributions of monomeric and dimeric receptors described here and in previously published studies. We performed superresolution imaging below the diffraction limit of light, which enabled the investigation of receptors on the plasma membrane of intact cells at an abundance similar to that of endogenous TLR4 (*20*). However, that TLR4 exhibited an increased tendency to exist as dimers in response to agonistic LPS is evident in both studies. Overall, our data provide information on the dimerization of TLR4 in intact cells, which we elucidated with SMLM. Future research on TLR4 and receptors that undergo oligomerization can use SMLM to obtain information on the oligomerization state and organization of the receptor. These findings will help to understand the pivotal start of signaling responses, which is often dependent on the change of the oligomeric state of the receptor.

MATERIALS AND METHODS

Cell culture

HEK 293 cells (a gift from H. Niemann, Bielefeld University) and HEK293_CD14MD2 cells (InvivoGen) were cultured at 37°C and 5% CO_2 in Dulbecco's modified Eagle medium (DMEM; Life Technologies) supplemented with 1% GlutaMAX (Gibco) and 10% fetal bovine serum (FBS; Capricorn Scientific). For luciferase assays, DMEM, GlutaMAX, and FBS were sourced from Sigma-Aldrich (FBS lot: 126K3398).

Cleaning and coating of microscopy slides

Glass slides (PLANO GmbH) were used for the imaging of transfected cells. Slides were incubated in isopropyl alcohol (Sigma-Aldrich) for 30 min, rinsed with endotoxin-free water, dried, and plasma-cleaned with N_2 (Diener Electronic) for 15 min. Slides were then coated for 1 hour with polyethylene glycol (PEG; Rapp Polymere) covalently coupled at either end to poly-L-lysine (PLL; Sigma-Aldrich) and a peptide containing the RGD-binding motif [PLL-PEG-RGD (*64*); 0.8 mg/ml], washed extensively with endotoxin-free water, and dried with N_2.

Plasmids

A plasmid encoding hTLR4 with the complementary DNA (cDNA) encoding mEos2 fused to the C terminus was generated by standard cloning techniques. Three inserts were generated as follows. First, part of the cytomegalovirus (CMV) promoter and the 5′ end of hTLR4 was excised at the Nde I and Hpa II sites from pRP-CMV-hTLR4-mEos3.2 (generated by Cyagen Biosciences). Second, the stop codon of hTLR4 was removed by polymerase chain reaction using the following primers: 5′-GGAATGAGCTAGTAAAGAATTTAGA-3′ (forward) and 5′-TGGCAGGAAGCAACATCTATCCTCGAGTATATA-3′ (reverse). The product was then digested with Hpa II and Xho I. Third, the sequence encoding mEos2 was removed from pRSETa-mEos2 (a gift from L. Looger; Addgene plasmid #20341) at the Xho I and Not I sites. The plasmid pcDNA3.1(+) was digested with Nde I and Not I, and the three inserts were ligated to generate pcDNA3.1-hTLR4-mEos2. The plasmids encoding the monomeric CD86_mEos2 protein and the dimeric CTLA-4_mEos2 protein were described previously (*34*).

Cell transfections

For transfections, cells were seeded in six-well plates and cultured until ~90% confluent. Lipofectamine 3000 (Thermo Fisher Scientific) was used according to the manufacturer's guidelines to transfect the cell lines with plasmids encoding TLR4_mEos2, CD86_mEos2, or CTLA-4_mEos2, as appropriate (2.5 μg of endotoxin-free plasmid was used per transfection). Cells were then kept in phenol red–free medium, replated on cleaned and coated glass slides, and cultured overnight in the incubator to adhere before they were starved in FBS-free medium for at least 4 hours. For the luciferase measurements, HEK293_CD14MD2 cells were transfected 4 hours before serum starvation with endotoxin-free TK (NF-κB$_6$) LUC (for NF-κB reporter gene assay) or with IRF-3-Gal4 (pEFGal4-IRF-3) and UAS-LUC (p55UASGLuc), both provided by K. Fitzgerald, University of Massachusetts Medical School (for the IRF3 reporter gene assay), pcDNA3.1-hTLR4-mEos2, and pRL-CMV (1:1:2 ratio; Promega Corporation) with TurboFect Transfection Reagent (Thermo Fisher Scientific) according to the manufacturer's guidelines. To test TLR4 functionality, the cells were transfected with plasmids encoding EGFP, TLR4_GFP (InvivoGen) (*65*), or TLR4_mEOS2.

LPS treatment

After the cells were subjected to serum starvation, LPS$_{EC}$ (ultrapure *E. coli* K12, InvivoGen) or LPS$_{SM}$ (ultrapure *S. minnesota* R595, InvivoGen) was applied to the cells in FBS-containing medium for 30 min (each at a final concentration of 1 μg/ml). For experiments with LPS$_{RS}$ (ultrapure *R. sphaeroides*, InvivoGen), LPS (10 μg/ml) was added to the serum-free medium, and the cells were treated for 8 hours. The concentration of LPS$_{RS}$ was chosen to ensure complete antagonism of TLR4 (*22*). All LPS chemotypes were ultrapure, dissolved in endotoxin-free water, and sonicated for at least 5 min before being used. As a control, cells were not treated with any LPS chemotype. After LPS treatment, the cells were washed with prewarmed 400 mM sucrose in phosphate-buffered saline (PBS) and afterward incubated for 15 min with fixation buffer [4% formaldehyde (methanol-free), Thermo Fisher Scientific], 0.2% glutaraldehyde (Sigma-Aldrich), and 400 mM sucrose in PBS. Samples were then washed extensively in PBS. Fixation of HEK 293 cells expressing CD86_mEos2 or CTLA-4_mEos2 was performed as described earlier with no previous stimulation with LPS. For the luciferase measurements, cells were serum-starved for 4 hours with or without LPS$_{RS}$ (10 μg/ml). The cells were then left untreated or were treated with LPS$_{RS}$ (10 μg/ml) for 48 hours in normal culture medium containing ultrapure LPS derived from *S. minnesota* or *E. coli* (1 μg/ml). Untreated cells and cells exposed to LPS$_{RS}$ alone served as controls.

Luciferase measurement

NF-κB reporter activation and IRF3 reporter activation (*firefly* luciferase activity) versus *Renilla* luciferase activity were examined with a Dual-Luciferase Reporter Assay System (Promega Corporation) according to the manufacturer's guidelines. All luciferase measurements were performed with a Lucy 1 microplate reader (Anthos Labtec).

Single-molecule localization microscopy

For SMLM measurements of TLR4_mEos2 in HEK 293 or HEK293_CD14MD2 cells and measurements of the calibration proteins (CD86_mEos2 and CTLA-4_mEos2) in HEK 293 cells, a custom-built setup was used as previously described (*34*). Briefly, a 568-nm laser (Sapphire 568 LP, Coherent) and a 405-nm UV laser (Cube 405-50C, Coherent) were focused on the back focal plane of an Olympus IX71 inverted microscope equipped with a 100× oil immersion objective [PLAPO 100×O TIRFM (NA 1.45), Olympus] and dichroic mirrors (AHF). To minimize drift, a "nose piece" (Olympus) was mounted onto the objective, which maintained the distance between the sample and the objective. Fluorescence was detected with an EMDDC camera (iXon3 and iXon Ultra, Andor) after filtering with a bandpass (BrightLine HC 590/20, AHF). Samples were imaged in PBS. Recording was started before the cells were illuminated with the 568-nm laser and a UV laser. Imaging was performed in TIRF mode with a frame rate of 10 Hz and under continuous 568-nm laser illumination (0.5 kW/cm^2) and increasing UV illumination (0 to 10 W/cm^2) until no further blinking events were observed.

SMLM analysis

Superresolved images of TLR4_mEos2, CD86_mEos2, and CTLA-4_mEos2 were reconstructed with rapi*d*STORM and custom-written software [LAMA (LocAlization Microscopy Analyzer)] (*66*, *67*). In rapi*d*STORM, images were reconstructed and a localization list was generated; localizations that appeared with a brightness of less than 63 photons were not taken into account. Signals from mEos2, which appeared in consecutive camera frames within a radius of 90 nm, were grouped together as a single localization by a Kalman filtering routine. The localization precision was determined with a NeNa (*48*). To exclude mEos2 particles that may not have photobleached until the end of the experiment, we excluded all clusters from the analysis that showed blinking events in the last 1000 frames of the image stack. This ensured that the blinking statistics were not distorted by clusters with incomplete blinking cycles. For oligomerization analysis, the number of blinking events was extracted from individual mEos2 clusters; clusters with a low brightness, a diameter greater than 120 nm, or low circularity, as well as clusters with any localization nearby (a distance of at least 60 nm) were discarded (Fig. 1). At least 500 clusters per condition were analyzed. For each condition, at least nine different cells were taken into account from at least four independent experiments per condition. Frequency distributions of the number of blinking events were approximated by fitting functions, which describe the blinking statistics of simple fluorophores (*39*). For example, the blinking statistics of a monomer (one fluorophore) is given by:

$$p_0(n) = p(1-p)^n \quad (1)$$

The blinking statistics of a dimer is given by:

$$p_1(n) = p(1-p)^{n-1} p(1-q)n + (1-p)q \quad (2)$$

whereas the blinking statistics of a mixed population of monomers and dimers is given by:

$$p_{0/1} = p(1-p)^n f + (1-f)p\left((1-p)^{(n-1)}\right)\left(p(1-q)n + (1-p)q\right) \quad (3)$$

We used the parameters p and q, where p describes the fraction of fluorophores that did not undergo blinking after initial photoactivation, q describes the fraction of damaged, undetected fluorophores, and f describes the fraction of monomeric protein within a mixed population (*39*). To analyze a mixed population of monomers and dimers, we used a weighted average. Only cells with low quantities of exogenous protein were used for analysis to avoid artifacts due to overexpression and to minimize the chance of overlapping blinking fluorophores.

Statistical analysis

Statistical analysis was performed with GraphPad Prism software (GraphPad). Data are shown as means ± SEM of at least three independent measurements and were compared by one-way ANOVA with Bonferroni correction (with a confidence interval of 95%). A P value of <0.05 was considered statistically significant.

REFERENCES AND NOTES

1. K. Takeda, S. Akira, Toll-like receptors in innate immunity. *Int. Immunol.* **17**, 1–14 (2005).
2. J. C. Chow, D. W. Young, D. T. Golenbock, W. J. Christ, F. Gusovsky, Toll-like receptor-4 mediates lipopolysaccharide-induced signal transduction. *J. Biol. Chem.* **274**, 10689–10692 (1999).
3. B. Beutler, Tlr4: Central component of the sole mammalian LPS sensor. *Curr. Opin. Immunol.* **12**, 20–26 (2000).
4. R. J. Ulevitch, P. S. Tobias, Receptor-dependent mechanisms of cell stimulation by bacterial endotoxin. *Annu. Rev. Immunol.* **13**, 437–457 (1995).
5. R. R. Schumann, S. R. Leong, G. W. Flaggs, P. W. Gray, S. D. Wright, J. C. Mathison, P. S. Tobias, R. J. Ulevitch, Structure and function of lipopolysaccharide binding protein. *Science* **249**, 1429–1431 (1990).
6. K. A. Fitzgerald, D. C. Rowe, B. J. Barnes, D. R. Caffrey, A. Visintin, E. Latz, B. Monks, P. M. Pitha, D. T. Golenbock, LPS-TLR4 signaling to IRF-3/7 and NF-κB involves the Toll adapters TRAM and TRIF. *J. Exp. Med.* **198**, 1043–1055 (2003).
7. C. R. Casella, T. C. Mitchell, Putting endotoxin to work for us: Monophosphoryl lipid A as a safe and effective vaccine adjuvant. *Cell Mol. Life Sci.* **65**, 3231–3240 (2008).
8. T. Kawai, O. Adachi, T. Ogawa, K. Takeda, S. Akira, Unresponsiveness of MyD88-deficient mice to endotoxin. *Immunity* **11**, 115–122 (1999).
9. D. Widera, A. Kaus, C. Kaltschmidt, B. Kaltschmidt, Neural stem cells, inflammation and NF-κB: Basic principle of maintenance and repair or origin of brain tumours? *J. Cell. Mol. Med.* **12**, 459–470 (2008).
10. K. A. Fitzgerald, S. M. McWhirter, K. L. Faia, D. C. Rowe, E. Latz, D. T. Golenbock, A. J. Coyle, S.-M. Liao, T. Maniatis, IKKε and TBK1 are essential components of the IRF3 signaling pathway. *Nat. Immunol.* **4**, 491–496 (2003).
11. A. I. Dragan, V. V. Hargreaves, E. N. Makeyeva, P. L. Privalov, Mechanisms of activation of interferon regulator factor 3: The role of C-terminal domain phosphorylation in IRF-3 dimerization and DNA binding. *Nucleic Acids Res.* **35**, 3525–3534 (2007).
12. R. Shimazu, S. Akashi, H. Ogata, Y. Nagai, K. Fukudome, K. Miyake, M. Kimoto, MD-2, a molecule that confers lipopolysaccharide responsiveness on Toll-like receptor 4. *J. Exp. Med.* **189**, 1777–1782 (1999).
13. B. S. Park, D. H. Song, H. M. Kim, B.-S. Choi, H. Lee, J.-O. Lee, The structural basis of lipopolysaccharide recognition by the TLR4–MD-2 complex. *Nature* **458**, 1191–1195 (2009).
14. S.-i. Saitoh, S. Akashi, T. Yamada, N. Tanimura, M. Kobayashi, K. Konno, F. Matsumoto, K. Fukase, S. Kusumoto, Y. Nagai, Y. Kusumoto, A. Kosugi, K. Miyake, Lipid A antagonist, lipid IVa, is distinct from lipid A in interaction with Toll-like receptor 4 (TLR4)-MD-2 and ligand-induced TLR4 oligomerization. *Int. Immunol.* **16**, 961–969 (2004).
15. C. R. H. Raetz, C. Whitfield, Lipopolysaccharide endotoxins. *Annu. Rev. Biochem.* **71**, 635–700 (2002).
16. S. I. Miller, R. K. Ernst, M. W. Bader, LPS, TLR4 and infectious disease diversity. *Nat. Rev. Microbiol.* **3**, 36–46 (2005).
17. K. Brandenburg, M. H. J. Koch, U. Seydel, Phase diagram of lipid A from *Salmonella minnesota* and *Escherichia coli* rough mutant lipopolysaccharide. *J. Struct. Biol.* **105**, 11–21 (1990).
18. F. Peri, M. Piazza, Therapeutic targeting of innate immunity with Toll-like receptor 4 (TLR4) antagonists. *Biotechnol. Adv.* **30**, 251–260 (2012).
19. H. Loppnow, P. Libby, M. Freudenberg, J. H. Krauss, J. Weckesser, H. Mayer, Cytokine induction by lipopolysaccharide (LPS) corresponds to lethal toxicity and is inhibited by nontoxic *Rhodobacter capsulatus* LPS. *Infect. Immun.* **58**, 3743–3750 (1990).
20. M.-T. Zeuner, C. L. Krüger, K. Volk, K. Bieback, G. S. Cottrell, M. Heilemann, D. Widera, Biased signalling is an essential feature of TLR4 in glioma cells. *Biochim. Biophys. Acta* **1863**, 3084–3095 (2016).
21. H. M. Kim, B. S. Park, J.-I. Kim, S. E. Kim, J. Lee, S. C. Oh, P. Enkhbayar, N. Matsushima, H. Lee, O. J. Yoo, J.-O. Lee, Crystal structure of the TLR4-MD-2 complex with bound endotoxin antagonist Eritoran. *Cell* **130**, 906–917 (2007).
22. A. Visintin, K. A. Halmen, E. Latz, B. G. Monks, D. T. Golenbock, Pharmacological inhibition of endotoxin responses is achieved by targeting the TLR4 coreceptor, MD-2. *J. Immunol.* **175**, 6465–6472 (2005).
23. A. Fürstenberg, M. Heilemann, Single-molecule localization microscopy–near-molecular spatial resolution in light microscopy with photoswitchable fluorophores. *Phys. Chem. Chem. Phys.* **15**, 14919–14930 (2013).
24. E. Betzig, G. H. Patterson, R. Sougrat, O. W. Lindwasser, S. Olenych, J. S. Bonifacino, M. W. Davidson, J. Lippincott-Schwartz, H. F. Hess, Imaging intracellular fluorescent proteins at nanometer resolution. *Science* **313**, 1642–1645 (2006).
25. M. J. Rust, M. Bates, X. Zhuang, Sub-diffraction-limit imaging by stochastic optical reconstruction microscopy (STORM). *Nat. Methods* **3**, 793–795 (2006).
26. M. Heilemann, S. van de Linde, M. Schüttpelz, R. Kasper, B. Seefeldt, A. Mukherjee, P. Tinnefeld, M. Sauer, Subdiffraction-resolution fluorescence imaging with conventional fluorescent probes. *Angew. Chem. Int. Ed. Engl.* **47**, 6172–6176 (2008).
27. F. Fricke, S. Malkusch, G. Wangorsch, J. F. Greiner, B. Kaltschmidt, C. Kaltschmidt, D. Widera, T. Dandekar, M. Heilemann, Quantitative single-molecule localization microscopy combined with rule-based modeling reveals ligand-induced TNF-R1 reorganization toward higher-order oligomers. *Histochem. Cell Biol.* **142**, 91–101 (2014).
28. L. Tarancón Díez, C. Bönsch, S. Malkusch, Z. Truan, M. Munteanu, M. Heilemann, O. Hartley, U. Endesfelder, A. Fürstenberg, Coordinate-based co-localization-mediated analysis of arrestin clustering upon stimulation of the C–C chemokine receptor 5 with RANTES/CCL5 analogues. *Histochem. Cell Biol.* **142**, 69–77 (2014).
29. J. Lee, P. Sengupta, J. Brzostowski, J. Lippincott-Schwartz, S. K. Pierce, The nanoscale spatial organization of B-cell receptors on immunoglobulin M– and G–expressing human B-cells. *Mol. Biol. Cell* **28**, 511–523 (2016).
30. U. Endesfelder, K. Finan, S. J. Holden, P. R. Cook, A. N. Kapanidis, M. Heilemann, Multiscale spatial organization of RNA polymerase in *Escherichia coli*. *Biophys. J.* **105**, 172–181 (2013).
31. J. Wiedenmann, S. Ivanchenko, F. Oswald, F. Schmitt, C. Röcker, A. Salih, K.-D. Spindler, G. U. Nienhaus, EosFP, a fluorescent marker protein with UV-inducible green-to-red fluorescence conversion. *Proc. Natl. Acad. Sci. U.S.A.* **101**, 15905–15910 (2004).
32. S.-H. Lee, J. Y. Shin, A. Lee, C. Bustamante, Counting single photoactivatable fluorescent molecules by photoactivated localization microscopy (PALM). *Proc. Natl. Acad. Sci. U.S.A.* **109**, 17436–17441 (2012).
33. S. Avilov, R. Berardozzi, M. S. Gunewardene, V. Adam, S. T. Hess, D. Bourgeois, *In cellulo* evaluation of phototransformation quantum yields in fluorescent proteins used as markers for single-molecule localization microscopy. *PLOS ONE* **9**, e98362 (2014).
34. F. Fricke, J. Beaudouin, R. Eils, M. Heilemann, One, two or three? Probing the stoichiometry of membrane proteins by single-molecule localization microscopy. *Sci. Rep.* **5**, 14072 (2015).
35. S. Ferré, V. Casadó, L. A. Devi, M. Filizola, R. Jockers, M. J. Lohse, G. Milligan, J.-P. Pin, X. Guitart, G protein–coupled receptor oligomerization revisited: Functional and pharmacological perspectives. *Pharmacol. Rev.* **66**, 413–434 (2014).
36. J. Schlessinger, Receptor tyrosine kinases: Legacy of the first two decades. *Cold Spring Harb. Perspect. Biol.* **6**, a008912 (2014).
37. M. Atanasova, A. Whitty, Understanding cytokine and growth factor receptor activation mechanisms. *Crit. Rev. Biochem. Mol. Biol.* **47**, 502–530 (2012).
38. J. S. Aaron, B. D. Carson, J. A. Timlin, Characterization of differential Toll-like receptor responses below the optical diffraction limit. *Small* **8**, 3041–3049 (2012).
39. G. Hummer, F. Fricke, M. Heilemann, Model-independent counting of molecules in single-molecule localization microscopy. *Mol. Biol. Cell* **27**, 3637–3644 (2016).
40. V. Adam, K. Nienhaus, D. Bourgeois, G. U. Nienhaus, Structural basis of enhanced photoconversion yield in green fluorescent protein-like protein Dendra2. *Biochemistry* **48**, 4905–4915 (2009).
41. N. Durisic, L. Laparra-Cuervo, Á. Sandoval-Álvarez, J. S. Borbely, M. Lakadamyali, Single-molecule evaluation of fluorescent protein photoactivation efficiency using an in vivo nanotemplate. *Nat. Methods* **11**, 156–162 (2014).
42. M. H. Ulbrich, E. Y. Isacoff, Subunit counting in membrane-bound proteins. *Nat. Methods* **4**, 319–321 (2007).
43. S. Dorsch, K.-N. Klotz, S. Engelhardt, M. J. Lohse, M. Bünemann, Analysis of receptor oligomerization by FRAP microscopy. *Nat. Methods* **6**, 225–230 (2009).
44. J. R. James, M. I. Oliveira, A. M. Carmo, A. Iaboni, S. J. Davis, A rigorous experimental framework for detecting protein oligomerization using bioluminescence resonance energy transfer. *Nat. Methods* **3**, 1001–1006 (2006).
45. P. S. Linsley, S. G. Nadler, J. Bajorath, R. Peach, H. T. Leung, J. Rogers, J. Bradshaw, M. Stebbins, G. Leytze, W. Brady, A. R. Malacko, H. Marquardt, S.-Y. Shaw, Binding

stoichiometry of the cytotoxic T lymphocyte-associated molecule-4 (CTLA-4). A disulfide-linked homodimer binds two CD86 molecules. *J. Biol. Chem.* **270**, 15417–15424 (1995).
46. J. L. Greene, G. M. Leytze, J. Emswiler, R. Peach, J. Bajorath, W. Cosand, P. S. Linsley, Covalent dimerization of CD28/CTLA-4 and oligomerization of CD80/CD86 regulate T cell costimulatory interactions. *J. Biol. Chem.* **271**, 26762–26771 (1996).
47. E. M. Puchner, J. M. Walter, R. Kasper, B. Huang, W. A. Lim, Counting molecules in single organelles with superresolution microscopy allows tracking of the endosome maturation trajectory. *Proc. Natl. Acad. Sci. U.S.A.* **110**, 16015–16020 (2013).
48. U. Endesfelder, S. Malkusch, F. Fricke, M. Heilemann, A simple method to estimate the average localization precision of a single-molecule localization microscopy experiment. *Histochem. Cell Biol.* **141**, 629–638 (2014).
49. B. Huang, W. Wang, M. Bates, X. Zhuang, Three-dimensional super-resolution imaging by stochastic optical reconstruction microscopy. *Science* **319**, 810–813 (2008).
50. I. Parmryd, B. Önfelt, Consequences of membrane topography. *FEBS J.* **280**, 2775–2784 (2013).
51. M. B. Stone, S. A. Shelby, S. L. Veatch, Super-resolution microscopy: Shedding light on the cellular plasma membrane. *Chem. Rev.* **117**, 7457–7477 (2017).
52. C. Vaure, Y. Liu, A comparative review of Toll-like receptor 4 expression and functionality in different animal species. *Front. Immunol.* **5**, 316 (2014).
53. A. Burgert, S. Letschert, S. Doose, M. Sauer, Artifacts in single-molecule localization microscopy. *Histochem. Cell Biol.* **144**, 123–131 (2015).
54. F. A. Caetano, B. S. Dirk, J. H. K. Tam, P. C. Cavanagh, M. Goiko, S. S. G. Ferguson, S. H. Pasternak, J. D. Dikeakos, J. R. de Bruyn, B. Heit, MIiSR: Molecular interactions in super-resolution imaging enables the analysis of protein interactions, dynamics and formation of multi-protein structures. *PLOS Comput. Biol.* **11**, e1004634 (2015).
55. A. H. A. Clayton, S. G. Orchard, E. C. Nice, R. G. Posner, A. W. Burgess, Predominance of activated EGFR higher-order oligomers on the cell surface. *Growth Factors* **26**, 316–324 (2008).
56. M. Zeuner, K. Bieback, D. Widera, Controversial role of Toll-like receptor 4 in adult stem cells. *Stem Cell Rev.* **11**, 621–634 (2015).
57. C. Erridge, Endogenous ligands of TLR2 and TLR4: Agonists or assistants? *J. Leukoc. Biol.* **87**, 989–999 (2010).
58. J. A. Sloane, D. Blitz, Z. Margolin, T. Vartanian, A clear and present danger: Endogenous ligands of Toll-like receptors. *Neuromolecular Med.* **12**, 149–163 (2010).
59. S. S. Diebold, M. Montoya, H. Unger, L. Alexopoulou, P. Roy, L. E. Haswell, A. Al-Shamkhani, R. Flavell, P. Borrow, C. Reis e Sousa, Viral infection switches non-plasmacytoid dendritic cells into high interferon producers. *Nature* **424**, 324–328 (2003).
60. H. Uronen-Hansson, J. Allen, M. Osman, G. Squires, N. Klein, R. E. Callard, Toll-like receptor 2 (TLR2) and TLR4 are present inside human dendritic cells, associated with microtubules and the Golgi apparatus but are not detectable on the cell surface: Integrity of microtubules is required for interleukin-12 production in response to internalized bacteria. *Immunology* **111**, 173–178 (2004).
61. T. Shibata, Y. Motoi, N. Tanimura, N. Yamakawa, S. Akashi-Takamura, K. Miyake, Intracellular TLR4/MD-2 in macrophages senses Gram-negative bacteria and induces a unique set of LPS-dependent genes. *Int. Immunol.* **23**, 503–510 (2011).
62. Y. Yang, J. Wolfram, X. Fang, H. Shen, M. Ferrari, Polyarginine induces an antitumor immune response through binding to Toll-like receptor 4. *Small* **10**, 1250–1254 (2014).
63. R. J. Arant, M. H. Ulbrich, Deciphering the subunit composition of multimeric proteins by counting photobleaching steps. *Chemphyschem* **15**, 600–605 (2014).
64. S. VandeVondele, J. Vörös, J. A. Hubbell, RGD-grafted poly-L-lysine-*graft*-(polyethylene glycol) copolymers block non-specific protein adsorption while promoting cell adhesion. *Biotechnol. Bioeng.* **82**, 784–790 (2003).
65. F. Bachelerie, J. Alcami, F. Arenzana-Seisdedos, J.-L. Virelizier, HIV enhancer activity perpetuated by NF-κB induction on infection of monocytes. *Nature* **350**, 709–712 (1991).
66. S. Malkusch, M. Heilemann, Extracting quantitative information from single-molecule super-resolution imaging data with LAMA–LocAlization Microscopy Analyzer. *Sci. Rep.* **6**, 34486 (2016).
67. S. Wolter, A. Löschberger, T. Holm, S. Aufmkolk, M.-C. Dabauvalle, S. van de Linde, M. Sauer, rapi*d*STORM: Accurate, fast open-source software for localization microscopy. *Nat. Methods* **9**, 1040–1041 (2012).

Acknowledgments: We thank P. Freund for excellent technical assistance in cell culture and F. Fricke for help with data analysis. We thank H. Niemann (Bielefeld University) for providing us with HEK 293 cells and K. Fitzgerald (University of Massachusetts Medical School) for providing the IRF3 gene reporter system. **Funding:** The authors acknowledge funding by the German Science Foundation (DFG) (grants HE 6166/9-1 and WI4318/2-1). **Author contributions:** M.H. and D.W. conceived and designed the experiments. C.L.K., M.-T.Z., and G.S.C. performed the experiments. All authors analyzed the data and wrote the paper. **Competing interests:** The authors declare that they have no competing interests.

Submitted 8 March 2017
Accepted 13 October 2017
Published 31 October 2017
10.1126/scisignal.aan1308

Citation: C. L. Krüger, M.-T. Zeuner, G. S. Cottrell, D. Widera, M. Heilemann, Quantitative single-molecule imaging of TLR4 reveals ligand-specific receptor dimerization. *Sci. Signal.* **10**, eaan1308 (2017).